HHS Public Access

Author manuscript

Ocul Surf. Author manuscript; available in PMC 2023 April 01.

Published in final edited form as:

Ocul Surf. 2022 April ; 24: 1–11. doi:10.1016/j.jtos.2021.12.006.

Secreted Ly-6/uPAR-related protein-1 (SLURP1) is a pro-differentiation factor that stalls G1-S transition during corneal epithelial cell cycle progression

Sudha Swamynathan[1], **Gregory Campbell**[1], **Anil Tiwari**[1,~], **Shivalingappa K. Swamynathan**[1,2,3,4,*]

[1]Department of Ophthalmology, University of Pittsburgh School of Medicine, Pittsburgh

[2]McGowan Institute of Regenerative Medicine, University of Pittsburgh, Pittsburgh

[3]Fox Center for Vision Restoration, University of Pittsburgh, Pittsburgh

[4]Department of Cell Biology, University of Pittsburgh School of Medicine, Pittsburgh

Abstract

Purpose: Previously we demonstrated that the secreted Ly-6/uPAR related protein-1 (SLURP1), abundantly expressed in the corneal epithelium (CE) and secreted into the tear fluid, serves as an anti-inflammatory and anti-angiogenic molecule. Here we describe the *Slurp1*-null (*Slurp1X*−/−) mouse corneal phenotype for the first time.

Methods: We compared the 10-week-old wild type (WT) and *Slurp1X*−/− mouse corneal (*i*) histology by hematoxylin-eosin and periodic acid-Schiff's reagent staining, (*ii*) cell proliferation by immunostaining for Ki67, (*iii*) cell adhesion molecules by immunostaining for desmosomal and tight junction proteins, (*iv*) barrier function by fluorescein staining and (*v*) wound-healing by epithelial debridement. Effect of SLURP1 on cell cycle was quantified in human corneal limbal epithelial (HCLE) cells engineered to express SLURP1 (HCLE-SLURP1).

Results: WT and *Slurp1X*−/− corneal histology was largely comparable, other than a few loosely attached superficial cells in *Slurp1X*−/− corneas. Compared with the WT, *Slurp1X*−/− corneas displayed (*i*) increase in Ki67+ cells, (*ii*) altered expression and/or localization of tight junction proteins Tjp1 and Pard3, and desmosomal Dsp, (*iii*) increased superficial fragility and (*iv*) slower CE wound healing. HCLE-SLURP1 cells displayed (*i*) decrease in Ki67+ cells, (*ii*) increased cell number doubling time, (*iii*) stalling in G1-S phase transition during cell cycle, and (*iv*) downregulation of cyclins CCNE and CCND1/D2, cyclin-dependent kinases CDK4 and CDK6, and upregulation of CDK inhibitor p15/CDKN2B.

[*]Corresponding Author: Shivalingappa K. Swamynathan, Ph.D., University of Pittsburgh School of Medicine, 203 Lothrop Street, Room 1025, Pittsburgh, PA-15213. U.S.A., Phone: 412-802-6437, Fax: 412-647-5880, Swamynathansk@upmc.edu.
[~]Current Address: Dr. Shroff's Charitable Eye Hospital, New Delhi, India.

Disclosure: S. Swamynathan (Patent); S.K. Swamynathan, (Patent); (Patent number: 9,731,014 Issued in Aug 2017 Titled 'Use of SLURP1 as an Immunomodulatory Molecule in the Ocular Surface'). GC, None, AT, None.

Conclusions: Collectively, these results elucidate that *Slurp1X*−/− CE cell homeostasis is altered and suggest that SLURP1 is a pro-differentiation factor that stalls G1-S transition during cell cycle progression by downregulating cyclins and upregulating p15/CDKN2B.

Keywords

Cornea; Epithelium; SLURP1; Homeostasis; Proliferation; Differentiation

Introduction:

The cornea is a transparent, refractive tissue that protects the rest of the eye and enables proper focus of the incident light on the retina. It is comprised of three distinct cellular layers, each with unique functions and gene expression patterns. Characterization of the developmental changes in corneal gene expression identified several abundantly expressed genes whose functions had been relatively understudied [1, 2]. *SLURP1* which encodes the secreted Ly-6/uPAR-related protein-1 is one such gene that is highly abundantly expressed in the cornea, yet relatively understudied. SLURP1 belongs to the Ly6/uPAR family of proteins characterized by a three-finger structure with 5 disulfide bridges [3, 4]. It is expressed highly abundantly by the corneal epithelium (CE) and moderately in several other tissues, and secreted into the tear film, saliva and urine [1, 5–15]. SLURP1 is structurally related to the snake venom neurotoxin α-bungarotoxin, binds α7 subunit of the nicotinic acetylcholine receptor (α7nAchR), and regulates keratinocyte functions through the cholinergic pathways [11, 16]. SLURP1 is a late marker of epidermal differentiation [15], serves as a tumor suppressor [16, 17], and influences intracellular signal transduction, activation of the immune response, and cell adhesion, preventing tobacco nitrosamine-induced malignant transformation of oral cells [12, 13, 18–20]. In humans, mutations in *SLURP1* cause an autosomal recessive palmoplantar keratoderma (PPK) called Mal-de-Meleda [11, 15, 16, 19, 21–25]. *Slurp1X*−/− mice with a nonsense point mutation in exon 2 (N35X) that results in premature truncation of the protein mimicked this disease, and developed severe PPK with epidermal barrier defect, increased keratinocyte proliferation, and accumulation of lipid droplets in the stratum corneum [26]. Despite high expression of Slurp1 in the mouse cornea, *Slurp1X*−/− mouse eyes appeared grossly normal and the corresponding corneal phenotype was not characterized [26].

Immune privilege that enables the cornea to tolerate mild insults without eliciting acute inflammatory response depends on a diverse network of molecules [27–35]. Previously, we demonstrated that SLURP1 is one such immunomodulatory peptide that (*i*) is highly expressed in the CE and is downregulated upon exposure to pro-inflammatory insults [5], (*ii*) inhibits leukocyte infiltration into the healthy cornea, and is rapidly downregulated in pathogenic conditions, permitting protective inflammation to develop [6], (*iii*) acts as a soluble scavenger of urokinase-type plasminogen activator (uPA) [36], (*iv*) inhibits human umbilical vein endothelial cell (HUVEC) tube formation [37], (*v*) suppresses neutrophil chemotaxis and transmigration through confluent endothelial monolayer [38], and (*vi*) stabilizes epithelial cell junctions and suppresses TNF-α-induced cytokine production [39]. Taken together, these results demonstrated that SLURP1 plays an important role in corneal immunomodulation and CE homeostasis.

Though our previous work provided many useful leads [5, 6, 36–39]. our understanding of the ocular surface functions of SLURP1 and the underlying molecular mechanisms remained incomplete. Here, we attempted to fill this gap by evaluating the *Slurp1X*−/− mouse corneas in greater detail. Consistent with the corneal immune- and angiogenic-privilege being regulated by multiple redundant mechanisms, we found that the naïve 10-week-old *Slurp1X*−/− corneas do not display any spontaneous angiogenic inflammation. We also found that the *Slurp1X*−/− CE displays altered proliferation, adhesion, and migration, suggesting that the CE homeostasis is disrupted in the absence of Slurp1. Overexpression of SLURP1 in human corneal limbal epithelial (HCLE) cells resulted in decreased expression of cyclins, cyclin-dependent kinases (CDK) and increased expression of CDK inhibitor p15/CDKN2B, culminating in decreased proliferation. Based on these results, we suggest that SLURP1 is a pro-differentiation factor that promotes cell cycle arrest in G1-S transition by downregulating cyclins and upregulating p15/CDKN2B.

Materials and Methods

Breeding and Management of Mouse Strains.

Slurp1X−/− mice that carry a point mutation resulting in premature termination after 35 amino acids (N35X) in Slurp1 were a kind gift from Dr. Stephen Young, UCLA, and were re-derived in C57B1/6J background at the University of Pittsburgh [26]. The studies reported here conformed with the ARVO statement for the use of animals in ophthalmic and vision research and were performed in accordance with the University of Pittsburgh Institutional Animal Care and Use Committee guidelines (IACUC Protocol #: 21059346).

Histology.

Following carbon dioxide asphyxiation, eyes from ten-week-old WT and *Slurp1X*−/− mice were enucleated and fixed overnight in freshly prepared 4% paraformaldehyde in phosphate-buffered saline (PBS; pH 7.4) at room temperature, embedded in paraffin and sectioned in microtomes. Central corneal 8 μm-thick sections were stained with hematoxylin and eosin (H&E) or periodic acid and Schiff's reagent (PAS) following standard protocols, cover-slipped with Aqua-Poly/Mount (Polysciences, Warrington, PA), and imaged using an Olympus Bx60 microscope fitted with a Spot digital camera.

Isolation of RNA, Reverse Transcription and QPCR.

Total RNA was isolated from dissected mouse corneas using RNeasy columns (Qiagen, Germantown, MD), and cDNA was synthesized with mouse Moloney leukemia virus reverse transcriptase (Promega, Madison, WI). RT-QPCR assays were performed in duplicate in ABI StepOne Plus thermocycler using 18S rRNA or TBP as endogenous control with pre-standardized gene-specific primers (Applied Biosystems, Foster City, CA) or validated primers from IDT. At least five independent biological replicates were tested in each RT-QPCR experiment.

Cell Culture and Cell Cycle Analysis:

Human corneal limbal epithelial (HCLE) cells and those engineered to overexpress SLURP1 (HCLE-SLURP1) were cultured as described earlier [36, 40]. Single cell-derived clones

of HCLE cells infected with lentiviral particles carrying CMV promoter driven *SLURP1* gene were selected by blasticidin [36]. Based on immunoblots for SLURP1 expression, we selected HCLE-SLURP1-7 and HCLE-SLURP1-14 for moderate and high expression of SLURP1, respectively [36]. Doubling time for HCLE and HCLE-SLURP1 cells was calculated using xCELLigence Real-Time Cell Analysis (RTCA) instrument that uses cellular impedance to continuously monitor cell health, behavior, and function (Agilent Technologies, Santa Clara, CA). Equal number of cells were seeded in a 96-well e-plate and their growth monitored by xCELLigence System. Doubling time was derived from the exponential phase of the growth curve using RTCA Software Pro. For cell cycle analysis by flow cytometry, HCLE and HCLE-SLURP1 cells were seeded in 6-well plates to obtain around 60% confluence after 48 h of growth. Cells were harvested and fixed in 70% ethanol, re-suspended in PBS with RNAse-A, and stained with Propidium Iodide for FACS analysis. Data were collected on a FACSAria cytometer and analyzed using FlowJo software.

Immunoblots.

Equal amounts of total protein extracted using urea buffer or RIPA buffer were separated by sodium dodecyl sulfate-polyacrylamide gel electrophoresis (SDS-PAGE), electroblotted to polyvinylidene difluoride (PVDF) membranes and subjected to immunoblot analysis as described previously [38]. Equal loading was confirmed by stripping the blots of the antibody and re-probing them with anti-actin antibody. Densitometry was performed using Image-J (NIH) to quantify the immunoblot signal intensity [41]. Details of antibodies used in this study are provided in Supplemental Table-1.

Immunofluorescent Staining.

Eight μm-thick cryosections from optimal cutting temperature (OCT) compound-embedded eyes were fixed in freshly prepared 4% paraformaldehyde in PBS for 10 minutes, washed thrice for 5 minutes each with PBS, permeabilized with 0.1% triton when necessary and blocked for 1 h at room temperature with 10% goat or donkey serum in PBS, washed twice with PBS for 5 min each, followed by overnight incubations with primary antibody, washed thrice and an hour-long incubation with secondary antibody, counterstained with 4′,6-diamidino-2-phenylindole (DAPI), and cover-slipped with Aqua-Poly/Mount (Polysciences, Warrington, PA), dried overnight, sealed with clear nail polish, and imaged using an Olympus IX81 microscope and Olympus FluoView 1000 confocal system (Olympus, Center Valley, PA). HCLE cells grown on collagen-coated cover slips were fixed and stained as above.

For immunofluorescent staining of corneal whole mounts, dissected corneas were fixed overnight in 4% paraformaldehyde + 0.2% glutaraldehyde, blocked for 2 h in PBS + 10% goat serum, and incubated overnight with anti-Tjp1 antibody at 4°C. Corneas were then washed thrice each for 30 minutes in PBST, incubated with secondary antibody and DAPI for 2 h, washed thrice each for 30 minutes in PBST, flattened by three radial incisions, mounted in Aqua poly/Mount (Polysciences Inc, Warrington, PA) and imaged as above. All images presented within each composite figure were similarly acquired and processed using identical settings in Adobe Photoshop and Illustrator (Adobe, Mountain View, CA).

Corneal Epithelial Debridement Wounds.

Adult (PN-70) mice were anesthetized by intraperitoneal injection of ketamine/xylazine and topical application of proparacaine. Mild abrasion was performed by three circular swipes of cotton tipped applicators. Epithelial debridement wounds were generated with an Alger brush in the central corneal 1.5 mm diameter area demarcated by trephine blades. Wound area was stained with fluorescein, imaged under blue light using a biomicroscope, and the area measured using Image-J software (NIH).

Statistical Analyses.

All experiments described here were repeated at least thrice, and representative data or mean values from at least three independent repetitions are presented with standard error bars. For RT-QPCR and immunoblots, we have utilized 6 biological replicates. As immunofluorescent staining is a qualitative assay, we performed it with at least three replicates to ensure that the results are reproducible, remained consistent among replicates and aligned well with RT-QPCR and immunoblots. Student's t-test was used to measure statistical significance. When p values were less than 0.05, differences between treatments were deemed statistically significant.

Results

External appearance and histology of *Slurp1X−/−* eyes.

First, we confirmed the absence of *Slurp1* expression in *Slurp1X*−/− corneas by RT-QPCR, immunoblots and immunofluorescent stain (Fig. 1A–1C). External appearance of the naïve 10-week-old WT and *Slurp1X*−/− mouse eyes was comparable, with no major change or spontaneous angiogenic inflammation in the absence of Slurp1 (Fig. 2A). Histological examination of the H&E- and PAS reagent-stained sections revealed no major differences between the WT and *Slurp1X*−/− corneas other than the appearance of a few loosely held superficial cells in the *Slurp1X*−/− corneas (Fig. 2B and 2C). PAS reagent-stained sections also revealed that the *Slurp1X*−/− CE basement membrane is comparable to that in the WT (Fig. 2C). Comparison of total or soluble protein in the WT and *Slurp1X*−/− corneas isolated using urea buffer or RIPA buffer, respectively, and separated by SDS-PAGE also did not reveal any striking difference in their protein profiles (Supplemental Fig. 1). Taken together, these results suggest that the ablation of *Slurp1* causes no overt phenotypic change in the mouse cornea.

SLURP1 promotes G1-arrest by upregulating p15/CDKN2B and downregulating cyclins.

As previous work from our laboratory and others' suggested anti-proliferative property for SLURP1 [17, 42], we examined the proliferative status of *Slurp1X*−/− CE cells by staining for Ki67. Compared with the WT, *Slurp1X*−/− CE displayed higher number of Ki67+ cells in both the central and peripheral regions (Fig. 3). Ki67+ cells were also observed in the suprabasal cell layers in the *Slurp1X*−/− CE unlike those in the WT which were mostly restricted to the basal cell layers (Fig. 3). Consistent with these results, HCLE-SLURP1-7 and −14 cells engineered to express SLURP1 moderately and highly, respectively, under the control of CMV promoter [36] displayed significantly fewer Ki67+ cells compared

with the control HCLE cells (Fig. 4A & 4B). The average doubling time calculated using cellular impedance measurements in xCELLigence RTCA instrument was 16.3, 17.9 and 18.7 hours for HCLE, HCLE-SLURP1-7, and HCLE-SLURP1-14 cells, respectively (Fig. 4C). To better understand the effect of SLURP1 on cell cycle progression, we quantified the fraction of sub-confluent HCLE and HCLE-SLURP1 cells in different stages of cell cycle using flow analysis. HCLE cells that express low levels of SLURP1 had 63, 21 and 16 per cent cells in G1, S and G2 phase, respectively (Fig. 4D). In contrast, significantly larger fraction of HCLE-SLURP1-7 and −14 cells was arrested in G1 phase (74 and 82 %), with commensurate decrease in S (15 and 10 %) and G2 (11 and 8 %) phase, respectively (Fig. 4D).

To elucidate the molecular mechanisms responsible for G1-arrest of HCLE-SLURP1 cells, we examined the expression of different cell cycle regulators that control G1 to S phase transition during cell cycle progression. Immunoblots revealed that HCLE-SLURP1 cells expressed elevated levels of cyclin-dependent kinase inhibitor-2B (CDKN2B, also known as multiple tumor suppressor-2 (MTS-2) or $p15^{INK4b}$) (Fig. 5). In contrast, the expression of cyclin-E, cyclin-D1/D2 and CDKN2B-binding partners CDK4 and CDK6, was downregulated in HCLE-SLURP1 cells (Fig. 5). Collectively, these data suggest that SLURP1 promotes G1-arrest in HCLE cells by upregulating CDKN2B and downregulating cyclin-E, cyclin-D1/D2, CDK4 and CDK6, and that this regulation is disrupted in the *Slurp1X*−/− CE, resulting in their increased proliferation.

Altered healing of CE debridement wounds in *Slurp1X*−/− corneas.

Considering that (*i*) the *Slurp1X*−/− mouse epidermis displayed water barrier defect characteristic of palmoplantar keratoderma [26] and (*ii*) histology revealed that the superficial *Slurp1X*−/− CE cells are loosely attached (Fig. 2), we tested the effect of *Slurp1* ablation on CE barrier function. Fluorescein staining revealed that the barrier function of 10-week-old naïve *Slurp1X*−/− CE is comparable to that in the WT (Fig. 6A). However, *Slurp1X*−/− corneas displayed relatively increased fluorescein uptake upon mild abrasion with a cotton swab (Fig. 6B), suggesting that the *Slurp1X*−/− CE cells are loosely attached to each other, compared with the WT. As *Slurp1* ablation affected the CE cell proliferation (Fig. 3) and barrier (Fig. 6B), next we compared the migration of WT and *Slurp1X*−/− CE cells by CE debridement assays. *Slurp1X*−/− corneas only filled about 40% of the circular gaps created by CE debridement, unlike the WT corneas that efficiently covered about 85% of the gaps within 18 h of wounding (Fig. 6C). Together, these data suggest that the *Slurp1X*−/− CE displays fragile barrier and altered migration to fill debridement gaps.

Changes in cell-junction proteins in *Slurp1X*−/− CE.

Previously, we demonstrated that SLURP1 stabilizes cell junctions by promoting the expression of desmosomal cadherins [39]. As mild abrasions resulted in increased fluorescein uptake consistent with fragility in *Slurp1X*−/− CE (Fig. 6), next we tested the expression and localization of key cell junction molecules. RT-QPCR and immunoblots revealed no difference in the expression levels of Tjp1 (also called ZO1) in *Slurp1X*−/− corneas (Fig. 7A and 7B). However, whole-mount corneal immunofluorescent staining elucidated that Tjp1 is properly localized to the cell membranes in the WT CE (arrows),

but mis-localized to the nuclei in the superficial *Slurp1X*−/− CE cells (arrowheads; Fig. 7C). Immunofluorescent staining using cryosections also revealed decreased membrane localization of Tjp1 in the *Slurp1X*−/− CE suprabasal wing cells compared with the WT, with nuclear localization observed in a few superficial cells (Fig. 7D). RT-QPCR also revealed that the expression of transcripts that encode Par3, the apicobasal polarity (ABP) determinant that is localized to the tight junctions, was not altered in *Slurp1X*−/− corneas (Fig. 8A). However, immunoblots revealed a moderate reduction in both 200 kDa and 100 kDa isoforms of Par3 protein expression (Fig. 8B), and immunofluorescent staining revealed that Par3, like Tjp1, is prominently localized to the cell membranes in the WT, but not in the *Slurp1X*−/− CE cells, where it was diffusely localized in the cytoplasm (Fig. 8C). Finally, RT-QPCR revealed a significant decrease in transcripts encoding desmoplakin (Dsp), a key component of desmosomes (Fig. 9A). Consistent with these results, immunoblots and immunofluorescent staining confirmed that Dsp expression is significantly lower in *Slurp1X*−/− corneas (Fig. 9B and 9C). Collectively, these results elucidate that the expression and/or localization of key cell adhesion molecules is altered in the *Slurp1X*−/− CE.

Discussion

Previously, we reported that SLURP1, abundantly expressed by the CE and secreted into the tear film, serves as an anti-angiogenic and anti-inflammatory factor [5, 6, 36–39]. The data presented in this study elucidate that *Slurp1X*−/− mouse corneas (*i*) are histologically comparable to WT, other than the presence of relatively more loosely attached cells at the surface, (*ii*) have higher number of proliferating Ki67+ cells, (*iii*) close CE debridement wounds at a relatively slower pace, and (*iv*) display altered expression or localization of cell junction proteins Tjp1, Par3 and Dsp. Also, HCLE-SLURP1 cells displayed (*i*) decreased number of Ki67+ cells, (*ii*) stalling in G1-S phase transition during cell cycle, and (*iii*) downregulation of cyclins CCND1/D2, CCNE, cyclin-dependent kinases CDK4 and CDK6, and upregulation of CDK inhibitor p15/CDKN2B. Collectively, these results elucidate that the *Slurp1X*−/− CE cell homeostasis is altered and suggest that SLURP1 is a pro-differentiation factor that stalls G1-S transition during cell cycle progression by downregulating cyclins and CDKs, and upregulating p15/CDKN2B.

Though *Slurp1* represents the 11th most highly transcribed gene in the mouse cornea [1] and our previous studies ascribed an important immunomodulatory role for Slurp1 [5, 6, 36–38], studies reported here revealed only subtle changes in *Slurp1X*−/− corneal phenotype. Also, *Slurp1X*−/− corneal protein profile revealed no compensatory change in protein expression. Lack of overt phenotype including the absence of angiogenic inflammation in naïve *Slurp1X*−/− corneas is consistent with the corneal immune- and angiogenic-privilege being regulated by multiple redundant mechanisms [28, 30, 43].

The number of Ki67+ proliferating cells was increased in the *Slurp1X*−/− CE and decreased in HCLE-SLURP1 cells, suggesting that SLURP1 is an anti-proliferative protein. Cell cycle analysis showed higher percent of HCLE-SLURP1 cells in G1 phase compared with the WT. Expression of p15/CDKN2B was increased in HCLE-SLURP1 cells and that of cyclin-D1/D2, - E, CDK4 and CDK6 was decreased. Considering that p15/CDKN2B binds

CDK4 and CDK6, prevents their activation by cyclin D, and inhibits G1-S progression during cell cycle [44–46], it is conceivable that the increased expression of CDKN2B is responsible for decreased proliferation of HCLE-SLURP1 cells. Though *Slurp1X*−/− CE displayed increased number of Ki67+ cells, a commensurate change in the expression of these cell cycle regulators was not detected by immunoblots in *Slurp1X*−/− corneas (data not shown), where only a small fraction of cells in the basal layer divide. Collectively, these results from the *Slurp1X* −/− CE and HCLE-SLURP1 cells suggest that SLURP1 acts as a pro-differentiation factor by promoting cell cycle arrest in G1-S transition via downregulation of cyclins and CDKs, and upregulating p15/CDKN2B.

Compared with the WT, the *Slurp1X*−/− CE cells migrated slowly to repopulate the gaps created by CE debridement. This is in contrast with our prior data where HCLE-SLURP1 and HUVEC cells exposed to exogenous SLURP1 migrated slowly in gap-filling assays in vitro [36, 37]. A potential reason for this disparity is that the previous studies were performed in vitro on artificially coated surfaces, while the current studies were conducted in vivo. Thus, the current results are more likely to truly reflect the influence of Slurp1 on CE wound healing.

An important observation in this study is that the expression of cell junction proteins is altered in the *Slurp1X*−/− CE cells. Although naïve WT and *Slurp1X*−/− CE fluorescein uptake was comparable, the *Slurp1X*−/− CE was more fragile as its barrier function was easily disrupted upon mild abrasion. Furthermore, Dsp expression was downregulated in the *Slurp1X*−/− CE. These findings are consistent with the report that the *Slurp1X*−/− mice develop severe PPK characterized by increased keratinocyte proliferation and a water barrier defect [26], and our previous finding that SLURP1 stabilizes HCLE-SLURP1 cell junctions by promoting the expression of DSP, DSG and E-cadherin [39]. The data presented here reveal that the expression of *Par3* transcripts is unaltered in the absence of Slurp1. However, its localization is disrupted in the *Slurp1X*−/− CE. Considering that ABP plays a key role in CE homeostasis [47] and that Par3 is an important determinant of ABP, it is conceivable that the altered Par3 localization in the absence of Slurp1 affects CE ABP, that in turn disrupts the CE homeostasis. Additional data derived using scanning and transmission electron microscopy would be helpful in quantifying the *Slurp1X*−/− corneal superficial cell adherence and the density of desmosomes, respectively.

In dry eye disease, hyperosmolarity of the tear fluid induces CE barrier disruption and corneal inflammation in an IL-36α/IL-36RA/IL-38 signaling-dependent manner [48]. Considering that (*i*) SLURP1 stabilizes epithelial intercellular junctions and suppresses TNF-α-induced upregulation of inflammatory cytokines by suppressing NF-κB [39], (*ii*) SLURP1 is downregulated in the tear fluid collected from inflamed ocular surfaces [5], and (*iii*) the data presented in this manuscript elucidate that the *Slurp1X*−/− CE barrier function is compromised, it would be worthwhile evaluating if pro-inflammatory IL-36α expression is elevated and that of the antagonists IL-36RA and IL-38 is suppressed in the *Slurp1X*−/− CE, to further elucidate the role of SLURP1 in dry eye-associated inflammation.

Mutations in SLURP1- a secreted protein- causing PPK is rather unusual, as PPK typically develops due to defects in structural proteins like keratins and desmosomal components

[49]. Considering that DSP is a prominent component of desmosomes [50], and mutations in *DSP* cause PPK [51–53], it is conceivable that PPK in Mal de Meleda is primarily due to the altered expression of DSP. It would therefore be important to examine if the skin and ocular surface epithelia of Mal-de-Meleda patients display any change in the expression and/or functions of these cell junction proteins. Similarly, considering that SLURP1 is highly expressed in the cornea, it would be worthwhile examining the ocular surface of Mal-de-Meleda patients for any defects.

In summary, though external appearance, and histology of the naive *Slurp1X*−/− corneas were largely comparable to the WT, this study identified differences in cell proliferation and expression of Tjp1 and Dsp, that correlated with increased fragility and altered wound healing in *Slurp1X*−/− CE. The data presented here elucidate that *Slurp1X*−/− CE cell homeostasis is altered and suggest that SLURP1 is a pro-differentiation factor that stalls G1-S transition during cell cycle progression by downregulating cyclins and CDKs, and upregulating p15/CDKN2B. Whether *Slurp1X*−/− corneal mucin barrier [54, 55] and/or immune privilege [27, 43] is altered, and how *Slurp1X*−/− corneas respond to acute pathological challenges such as viral, bacterial, or fungal infections, chemical burns, or harmful physical insults such as UV radiations remains to be determined.

Supplementary Material

Refer to Web version on PubMed Central for supplementary material.

Acknowledgements

This study was supported by R01 EY 022898 (SKS), RO1 EY 031684 (SKS), unrestricted grants from Research to Prevent Blindness and the Eye and Ear Foundation of Pittsburgh to the Department of Ophthalmology, University of Pittsburgh School of Medicine, and was performed with the help of the (i) Tissue Culture and Histology, (ii) Cytology, and (iii) Imaging core modules supported by the NEI Core Grant P30 EY08098. The authors thank Dr. Stephen G. Young and Dr. Loren G. Fong, UCLA, for sharing the *Slurp1X*−/− mice, Ms. Kate Davoli for help with histology, and Dr. Gary Yam for lending xCELLigence RTCA instrument.

References

[1]. Norman B, Davis J, Piatigorsky J. Postnatal gene expression in the normal mouse cornea by SAGE. Invest Ophthalmol Vis Sci. 2004;45:429–40. [PubMed: 14744882]

[2]. Stephens DN, Klein RH, Salmans ML, Gordon W, Ho H, Andersen B. The Ets transcription factor EHF as a regulator of cornea epithelial cell identity. J Biol Chem. 2013;288:34304–24. [PubMed: 24142692]

[3]. Loughner CL, Bruford EA, McAndrews MS, Delp EE, Swamynathan S, Swamynathan SK. Organization, evolution and functions of the human and mouse Ly6/uPAR family genes. Hum Genomics. 2016;10:10. [PubMed: 27098205]

[4]. Adermann K, Wattler F, Wattler S, Heine G, Meyer M, Forssmann WG, et al. Structural and phylogenetic characterization of human SLURP-1, the first secreted mammalian member of the Ly-6/uPAR protein superfamily. Protein Sci. 1999;8:810–9. [PubMed: 10211827]

[5]. Swamynathan S, Delp EE, Harvey SA, Loughner CL, Raju L, Swamynathan SK. Corneal Expression of SLURP-1 by Age, Sex, Genetic Strain, and Ocular Surface Health. Invest Ophthalmol Vis Sci. 2015;56:7888–96. [PubMed: 26670825]

[6]. Swamynathan S, Buela KA, Kinchington P, Lathrop KL, Misawa H, Hendricks RL, et al. Klf4 regulates the expression of Slurp1, which functions as an immunomodulatory peptide in the mouse cornea. Invest Ophthalmol Vis Sci. 2012;53:8433–46. [PubMed: 23139280]

[7]. Matsumoto H, Shibasaki K, Uchigashima M, Koizumi A, Kurachi M, Moriwaki Y, et al. Localization of acetylcholine-related molecules in the retina: implication of the communication from photoreceptor to retinal pigment epithelium. PLoS One. 2012;7:e42841. [PubMed: 22880119]

[8]. Horiguchi K, Horiguchi S, Yamashita N, Irie K, Masuda J, Takano-Ohmuro H, et al. Expression of SLURP-1, an endogenous alpha7 nicotinic acetylcholine receptor allosteric ligand, in murine bronchial epithelial cells. J Neurosci Res. 2009;87:2740–7. [PubMed: 19396877]

[9]. Narumoto O, Horiguchi K, Horiguchi S, Moriwaki Y, Takano-Ohmuro H, Shoji S, et al. Down-regulation of secreted lymphocyte antigen-6/urokinase-type plasminogen activator receptor-related peptide-1 (SLURP-1), an endogenous allosteric alpha7 nicotinic acetylcholine receptor modulator, in murine and human asthmatic conditions. Biochem Biophys Res Commun. 2010;398:713–8. [PubMed: 20621062]

[10]. Moriwaki Y, Watanabe Y, Shinagawa T, Kai M, Miyazawa M, Okuda T, et al. Primary sensory neuronal expression of SLURP-1, an endogenous nicotinic acetylcholine receptor ligand. Neurosci Res. 2009;64:403–12. [PubMed: 19409425]

[11]. Mastrangeli R, Donini S, Kelton CA, He C, Bressan A, Milazzo F, et al. ARS Component B: structural characterization, tissue expression and regulation of the gene and protein (SLURP-1) associated with Mal de Meleda. Eur J Dermatol. 2003;13:560–70. [PubMed: 14721776]

[12]. Moriwaki Y, Yoshikawa K, Fukuda H, Fujii YX, Misawa H, Kawashima K. Immune system expression of SLURP-1 and SLURP-2, two endogenous nicotinic acetylcholine receptor ligands. Life Sci. 2007;80:2365–8. [PubMed: 17286989]

[13]. Arredondo J, Chernyavsky AI, Grando SA. SLURP-1 and −2 in normal, immortalized and malignant oral keratinocytes. Life Sci. 2007;80:2243–7. [PubMed: 17280689]

[14]. Kawashima K, Yoshikawa K, Fujii YX, Moriwaki Y, Misawa H. Expression and function of genes encoding cholinergic components in murine immune cells. Life Sci. 2007;80:2314–9. [PubMed: 17383684]

[15]. Favre B, Plantard L, Aeschbach L, Brakch N, Christen-Zaech S, de Viragh PA, et al. SLURP1 is a late marker of epidermal differentiation and is absent in Mal de Meleda. J Invest Dermatol. 2007;127:301–8. [PubMed: 17008884]

[16]. Arredondo J, Chernyavsky AI, Webber RJ, Grando SA. Biological effects of SLURP-1 on human keratinocytes. J Invest Dermatol. 2005;125:1236–41. [PubMed: 16354194]

[17]. Lyukmanova EN, Bychkov ML, Sharonov GV, Efremenko AV, Shulepko MA, Kulbatskii DS, et al. Human secreted proteins SLURP-1 and SLURP-2 control the growth of epithelial cancer cells via interactions with nicotinic acetylcholine receptors. Br J Pharmacol. 2018;175:1973–86. [PubMed: 29505672]

[18]. Arredondo J, Chernyavsky AI, Grando SA. Overexpression of SLURP-1 and −2 alleviates the tumorigenic action of tobacco-derived nitrosamine on immortalized oral epithelial cells. Biochem Pharmacol. 2007;74:1315–9. [PubMed: 17643396]

[19]. Chimienti F, Hogg RC, Plantard L, Lehmann C, Brakch N, Fischer J, et al. Identification of SLURP-1 as an epidermal neuromodulator explains the clinical phenotype of Mal de Meleda. Hum Mol Genet. 2003;12:3017–24. [PubMed: 14506129]

[20]. Grando SA. Basic and clinical aspects of non-neuronal acetylcholine: biological and clinical significance of non-canonical ligands of epithelial nicotinic acetylcholine receptors. J Pharmacol Sci. 2008;106:174–9. [PubMed: 18285656]

[21]. Eckl KM, Stevens HP, Lestringant GG, Westenberger-Treumann M, Traupe H, Hinz B, et al. Mal de Meleda (MDM) caused by mutations in the gene for SLURP-1 in patients from Germany, Turkey, Palestine, and the United Arab Emirates. Hum Genet. 2003;112:50–6. [PubMed: 12483299]

[22]. Fischer J, Bouadjar B, Heilig R, Huber M, Lefevre C, Jobard F, et al. Mutations in the gene encoding SLURP-1 in Mal de Meleda. Hum Mol Genet. 2001;10:875–80. [PubMed: 11285253]

[23]. Hu G, Yildirim M, Baysal V, Yerebakan O, Yilmaz E, Inaloz HS, et al. A recurrent mutation in the ARS (component B) gene encoding SLURP-1 in Turkish families with mal de Meleda: evidence of a founder effect. J Invest Dermatol. 2003;120:967–9. [PubMed: 12787122]

[24]. Marrakchi S, Audebert S, Bouadjar B, Has C, Lefevre C, Munro C, et al. Novel mutations in the gene encoding secreted lymphocyte antigen-6/urokinase-type plasminogen activator receptor-related protein-1 (SLURP-1) and description of five ancestral haplotypes in patients with Mal de Meleda. J Invest Dermatol. 2003;120:351–5. [PubMed: 12603845]

[25]. Ward KM, Yerebakan O, Yilmaz E, Celebi JT. Identification of recurrent mutations in the ARS (component B) gene encoding SLURP-1 in two families with mal de Meleda. J Invest Dermatol. 2003;120:96–8. [PubMed: 12535203]

[26]. Adeyo O, Allan BB, Barnes RH 2nd, Goulbourne CN, Tatar A, Tu Y, et al. Palmoplantar keratoderma along with neuromuscular and metabolic phenotypes in Slurp1-deficient mice. J Invest Dermatol. 2014;134:1589–98. [PubMed: 24499735]

[27]. Niederkorn JY, Stein-Streilein J. History and physiology of immune privilege. Ocul Immunol Inflamm. 2010;18:19–23. [PubMed: 20128645]

[28]. Azar DT. Corneal angiogenic privilege: angiogenic and antiangiogenic factors in corneal avascularity, vasculogenesis, and wound healing (an American Ophthalmological Society thesis). Trans Am Ophthalmol Soc. 2006;104:264–302. [PubMed: 17471348]

[29]. Hazlett LD, Hendricks RL. Reviews for immune privilege in the year 2010: immune privilege and infection. Ocul Immunol Inflamm. 2010;18:237–43. [PubMed: 20662654]

[30]. Barabino S, Chen Y, Chauhan S, Dana R. Ocular surface immunity: homeostatic mechanisms and their disruption in dry eye disease. Prog Retin Eye Res. 2012;31:271–85. [PubMed: 22426080]

[31]. Clements JL, Dana R. Inflammatory corneal neovascularization: etiopathogenesis. Semin Ophthalmol. 2011;26:235–45. [PubMed: 21958169]

[32]. Yamanaka O, Liu CY, Kao WW. Fibrosis in the anterior segments of the eye. Endocr Metab Immune Disord Drug Targets. 2010;10:331–5. [PubMed: 20925651]

[33]. Gronert K Resolution, the grail for healthy ocular inflammation. Exp Eye Res. 2010;91:478–85. [PubMed: 20637194]

[34]. Ambati BK, Nozaki M, Singh N, Takeda A, Jani PD, Suthar T, et al. Corneal avascularity is due to soluble VEGF receptor-1. Nature. 2006;443:993–7. [PubMed: 17051153]

[35]. Cursiefen C, Chen L, Saint-Geniez M, Hamrah P, Jin Y, Rashid S, et al. Nonvascular VEGF receptor 3 expression by corneal epithelium maintains avascularity and vision. Proc Natl Acad Sci U S A. 2006;103:11405–10. [PubMed: 16849433]

[36]. Swamynathan S, Swamynathan SK. SLURP-1 modulates corneal homeostasis by serving as a soluble scavenger of urokinase-type plasminogen activator. Invest Ophthalmol Vis Sci. 2014;55:6251–61. [PubMed: 25168896]

[37]. Swamynathan S, Loughner CL, Swamynathan SK. Inhibition of HUVEC tube formation via suppression of NFkappaB suggests an anti-angiogenic role for SLURP1 in the transparent cornea. Exp Eye Res. 2017;164:118–28. [PubMed: 28803936]

[38]. Swamynathan S, Tiwari A, Loughner CL, Gnalian J, Alexander N, Jhanji V, et al. The secreted Ly6/uPAR-related protein-1 suppresses neutrophil binding, chemotaxis, and transmigration through human umbilical vein endothelial cells. Sci Rep. 2019;9:5898. [PubMed: 30976100]

[39]. Campbell G, Swamynathan S, Tiwari A, Swamynathan SK. The secreted Ly-6/uPAR related protein-1 (SLURP1) stabilizes epithelial cell junctions and suppresses TNF-alpha-induced cytokine production. Biochem Biophys Res Commun. 2019.

[40]. Argueso P, Tisdale A, Spurr-Michaud S, Sumiyoshi M, Gipson IK. Mucin characteristics of human corneal-limbal epithelial cells that exclude the rose bengal anionic dye. Invest Ophthalmol Vis Sci. 2006;47:113–9. [PubMed: 16384952]

[41]. Schneider CA, Rasband WS, Eliceiri KW. NIH Image to ImageJ: 25 years of image analysis. Nat Methods. 2012;9:671–5. [PubMed: 22930834]

[42]. Lyukmanova EN, Shulepko MA, Bychkov ML, Shenkarev ZO, Paramonov AS, Chugunov AO, et al. Human SLURP-1 and SLURP-2 Proteins Acting on Nicotinic Acetylcholine Receptors Reduce Proliferation of Human Colorectal Adenocarcinoma HT-29 Cells. Acta Naturae. 2014;6:60–6. [PubMed: 25558396]

[43]. Foulsham W, Coco G, Amouzegar A, Chauhan SK, Dana R. When Clarity Is Crucial: Regulating Ocular Surface Immunity. Trends Immunol. 2018;39:288–301. [PubMed: 29248310]

[44]. Latres E, Malumbres M, Sotillo R, Martin J, Ortega S, Martin-Caballero J, et al. Limited overlapping roles of P15(INK4b) and P18(INK4c) cell cycle inhibitors in proliferation and tumorigenesis. EMBO J. 2000;19:3496–506. [PubMed: 10880462]

[45]. Hannon GJ, Beach D. p15INK4B is a potential effector of TGF-beta-induced cell cycle arrest. Nature. 1994;371:257–61. [PubMed: 8078588]

[46]. Reynisdottir I, Polyak K, Iavarone A, Massague J. Kip/Cip and Ink4 Cdk inhibitors cooperate to induce cell cycle arrest in response to TGF-beta. Genes Dev. 1995;9:1831–45. [PubMed: 7649471]

[47]. Tiwari A, Swamynathan S, Jhanji V, Swamynathan SK. KLF4 Coordinates Corneal Epithelial Apical-Basal Polarity and Plane of Cell Division and Is Downregulated in Ocular Surface Squamous Neoplasia. Invest Ophthalmol Vis Sci. 2020;61:15.

[48]. Li JM, Lu R, Zhang Y, Lin J, Hua X, Pflugfelder SC, et al. IL-36alpha/IL-36RA/IL-38 signaling mediates inflammation and barrier disruption in human corneal epithelial cells under hyperosmotic stress. Ocul Surf. 2021;22:163–71. [PubMed: 34428579]

[49]. Sakiyama T, Kubo A. Hereditary palmoplantar keratoderma “clinical and genetic differential diagnosis”. J Dermatol. 2016;43:264–74. [PubMed: 26945534]

[50]. Mueller H, Franke WW. Biochemical and immunological characterization of desmoplakins I and II, the major polypeptides of the desmosomal plaque. J Mol Biol. 1983;163:647–71. [PubMed: 6341602]

[51]. Yao JV, Winship I. More than meets the eye: Palmoplantar keratoderma and arrhythmogenic right ventricular cardiomyopathy in a patient with loss of the DSP gene. JAAD Case Rep. 2020;6:804–6. [PubMed: 32875024]

[52]. Abi Zamer B, Mahfood M, Saleh B, Al Mutery AF, Tlili A. Novel mutation in the DSG1 gene causes autosomal-dominant striate palmoplantar keratoderma in a large Syrian family. Ann Hum Genet. 2019;83:472–6. [PubMed: 31192455]

[53]. Xue K, Zheng Y, Cui Y. A novel heterozygous missense mutation of DSP in a Chinese Han pedigree with palmoplantar keratoderma. J Cosmet Dermatol. 2019;18:371–6. [PubMed: 29607617]

[54]. Baudouin C, Rolando M, Benitez Del Castillo JM, Messmer EM, Figueiredo FC, Irkec M, et al. Reconsidering the central role of mucins in dry eye and ocular surface diseases. Prog Retin Eye Res. 2019;71:68–87. [PubMed: 30471351]

[55]. Martinez-Carrasco R, Argueso P, Fini ME. Membrane-associated mucins of the human ocular surface in health and disease. Ocul Surf. 2021;21:313–30. [PubMed: 33775913]

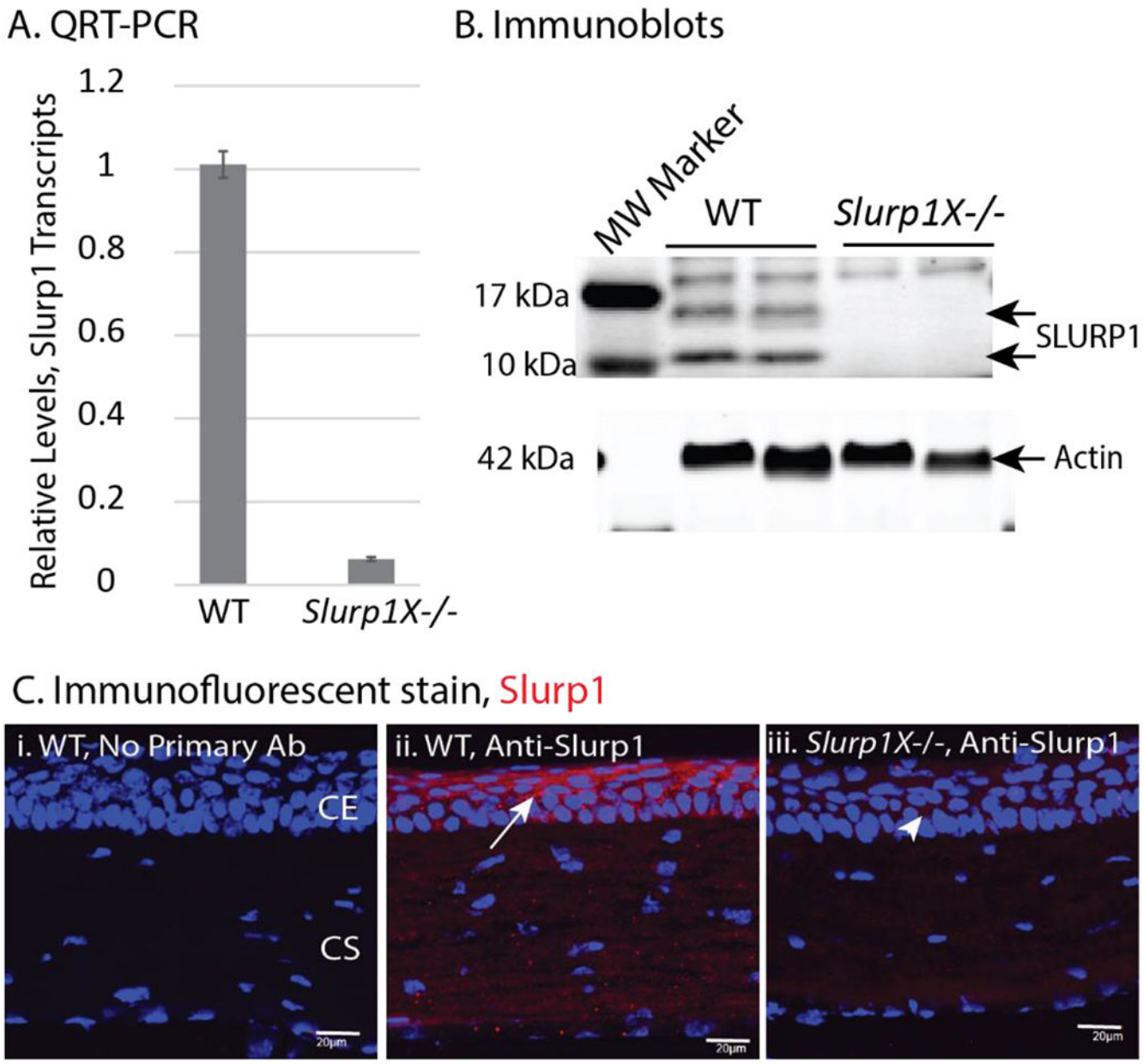

Figure 1. Confirmation of *Slurp1* ablation in *Slurp1X*−/− mouse corneas.

A. RT-QPCR reveals sharp decrease in *Slurp1* transcripts in the 10-week-old *Slurp1X*−/− corneas compared with the WT (n=5). B. Immunoblots reveal Slurp1 expression in the WT, but not the *Slurp1X*−/− corneas (n=6). C. Immunofluorescent stain confirmed the expression of Slurp1 in the WT CE (arrow) but not the *Slurp1X*−/− mouse CE. Magnification: 40X; Scale bar, 20 μm (n=6).

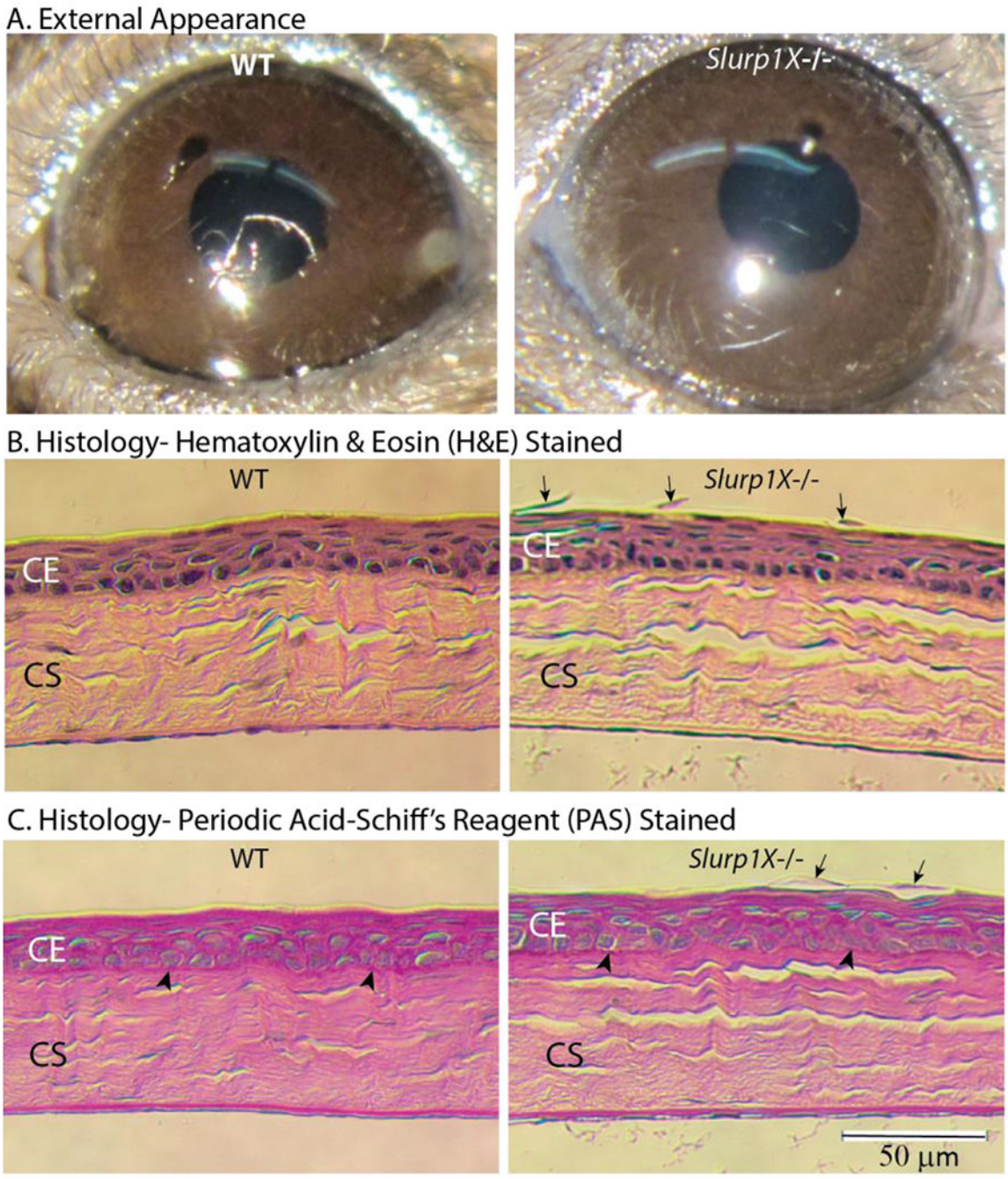

Figure 2. External appearance of the WT and *Slurp1X*−/− mouse eyes and histology of corresponding corneas.

A. External appearance of the WT and *Slurp1X*−/− mouse eyes imaged using a biomicroscope. B and C. Bright field image of (B) hematoxylin and eosin (H&E)- or (C) periodic acid-Schiff's reagent (PAS)-stained 8 µm thick section from paraformaldehyde-fixed, paraffin-embedded WT and *Slurp1X*−/− mouse eyeballs (n = at least 6). Loosely attached cells in the *Slurp1X*−/− CE are indicated by arrows. Arrowheads in C indicate the CE basement membrane stained by PAS reagent. CE, corneal epithelium; CS, corneal stroma. Magnification: 40X; Scale bar, 50 µm.

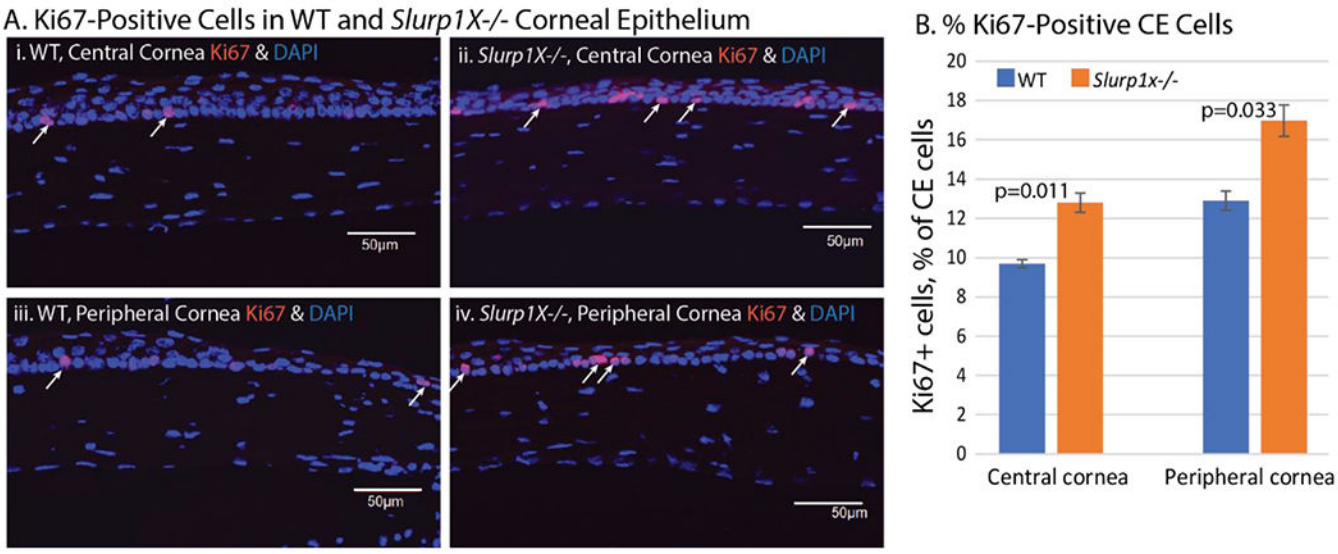

Figure 3. Ki67-positive cells in the WT and *Slurp1X*−/−central and peripheral corneas.

A. Immunofluorescent stain with anti-Ki67 antibody (red) shows increased number of Ki67+ cells in the *Slurp1X*−/− corneal central (top panels) and peripheral regions (bottom panels). Representative images are shown in A, and the mean number of Ki67+ cells derived from 6 biological replicates is shown in B, as percent of total CE cells (counted using DAPI stained nuclei; blue) in each microscopic field. Magnification: 20X; Scale bar, 50 μm (n=6).

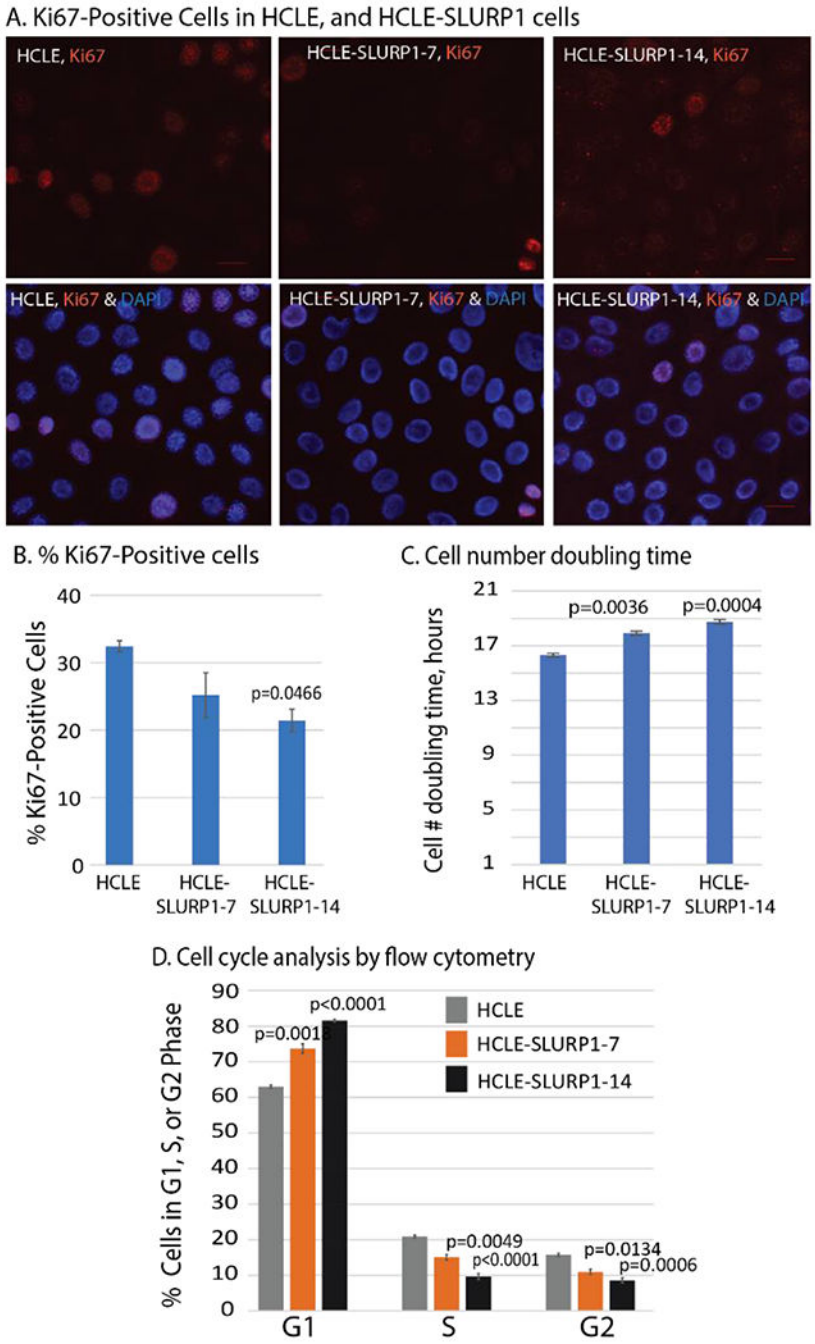

Figure 4. Ki67-positive cells in the HCLE and HCLE-SLURP1 cells.

A. Representative images showing Ki67+ cells in the HCLE, HCLE-SLURP1-7 and HCLE-SLURP1-14 cells. B. Mean number of Ki67+ cells, shown as percent of total cells counted using DAPI (blue) stain. Magnification: 40X. C. Cell number doubling time for HCLE and HCLE-SLURP1 cells quantified using xCELLigence RTCA instrument based on real-time cellular impedance measurements. Mean data from 3 independent experiments each with two replicates is shown. D. Mean percent of HCLE, HCLE-SLURP1-7 and HCLE-SLURP1-14 cells in G1, S or G2 phase of cell cycle, analyzed by flow cytometry. Compared

with the HCLE, higher percent of HCLE-SLURP1 cells were arrested in G1 phase, resulting in relatively lower percent in S and G2 phase of cell cycle. Data shown is an average from 3 independent experiments with 3 replicates in each. Corresponding p values are shown.

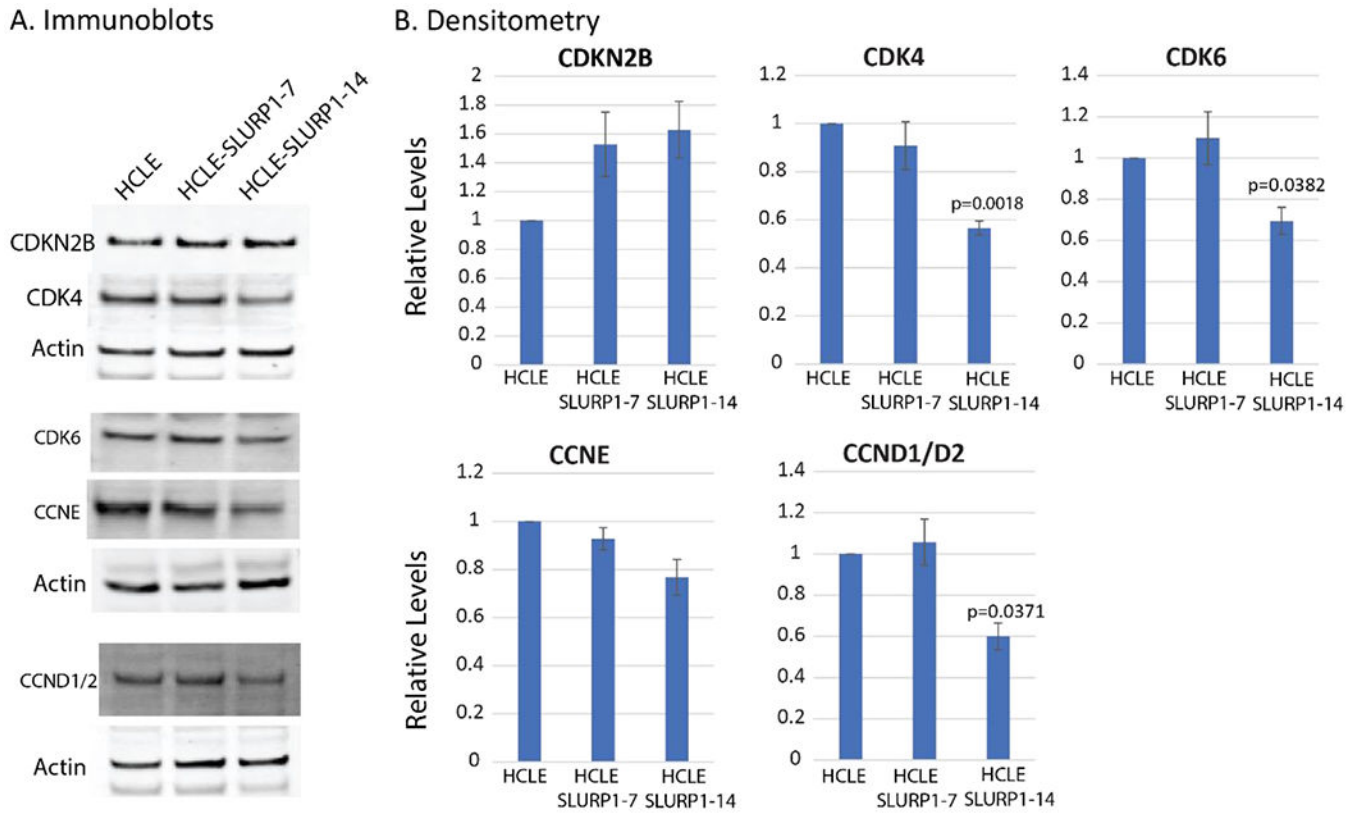

Figure 5. Expression of cell cycle regulators in the HCLE and HCLE-SLURP1 cells.

A. HCLE and HCLE-SLURP1 cell lysates prepared using RIPA buffer were separated by SDS-PAGE, electroblotted to PVDF membranes and probed with specific antibodies indicated. The blots were stripped of the primary antibody and re-probed with anti-actin antibody. Representative immunoblots for P15/CDKN2B, CDK6, CCNE and CCND1/D2, and corresponding actin levels are shown. B. Mean relative levels of different cell cycle regulators, calculated using densitometry from three independent experiments performed using different cell lysates is shown (n=3). P values are shown where significant.

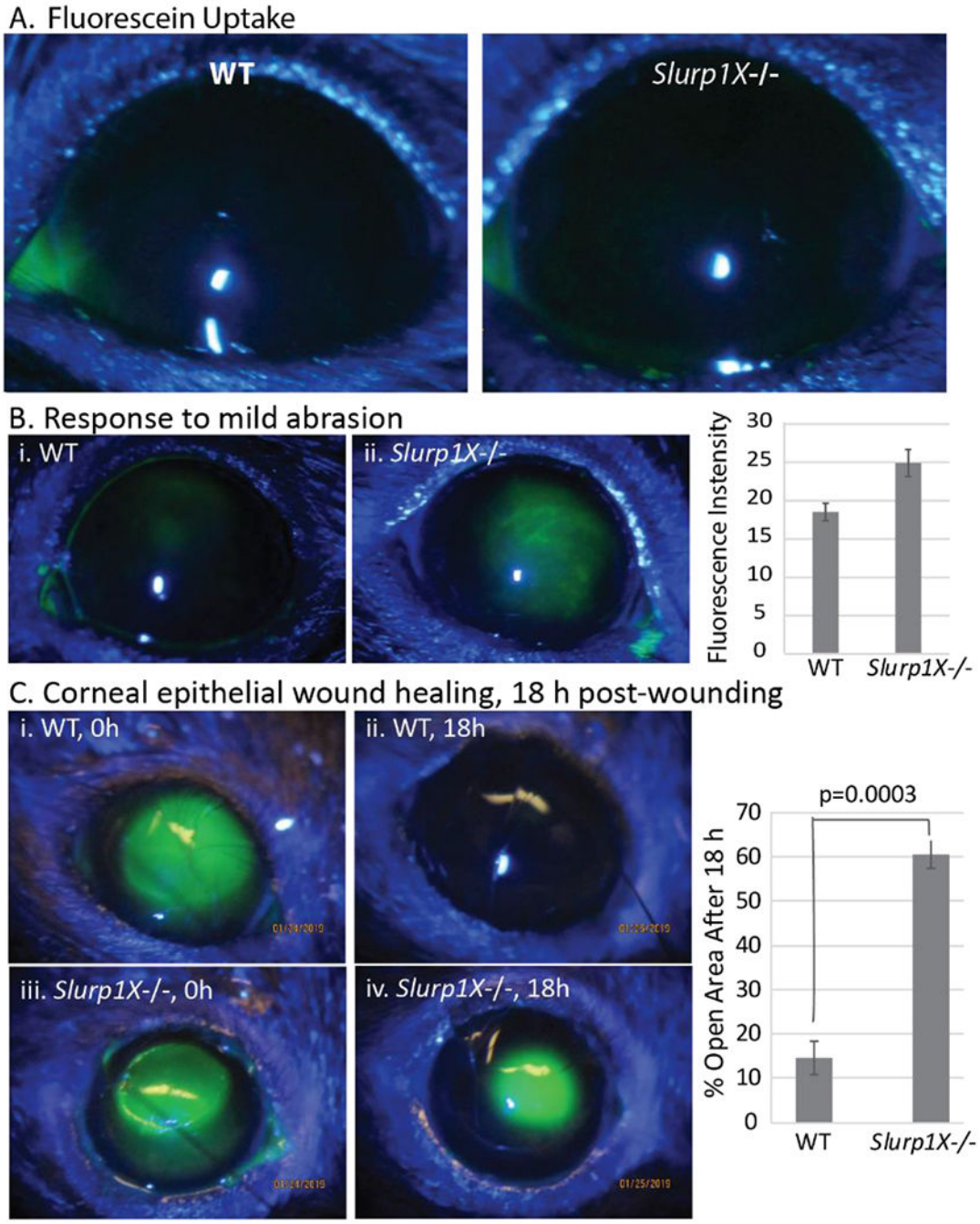

Figure 6. Compromised *Slurp1X*−/− CE barrier function and delayed wound healing.

A. WT and *Slurp1X*−/− eyes were stained with fluorescein and imaged under blue light. Representative images are shown (n>6). B. WT and *Slurp1X*−/− mouse eyes were subjected to mild abrasion with three circular swipes of a cotton tipped applicator and immediately stained with fluorescein as above. Representative images are shown with mean fluorescence intensity in adjoining bar diagram (n=15). C. Alger brush was used to debride an area of 1.5 mm diameter on WT and *Slurp1X*−/− mouse corneas, stained with fluorescein and imaged. Representative images of fluorescein-stained CE wounds at 0 and 18 h post-wounding are

shown. The mean remaining wound area at 18 h is shown in adjoining bar diagram as percent of total wounded area (n=8).

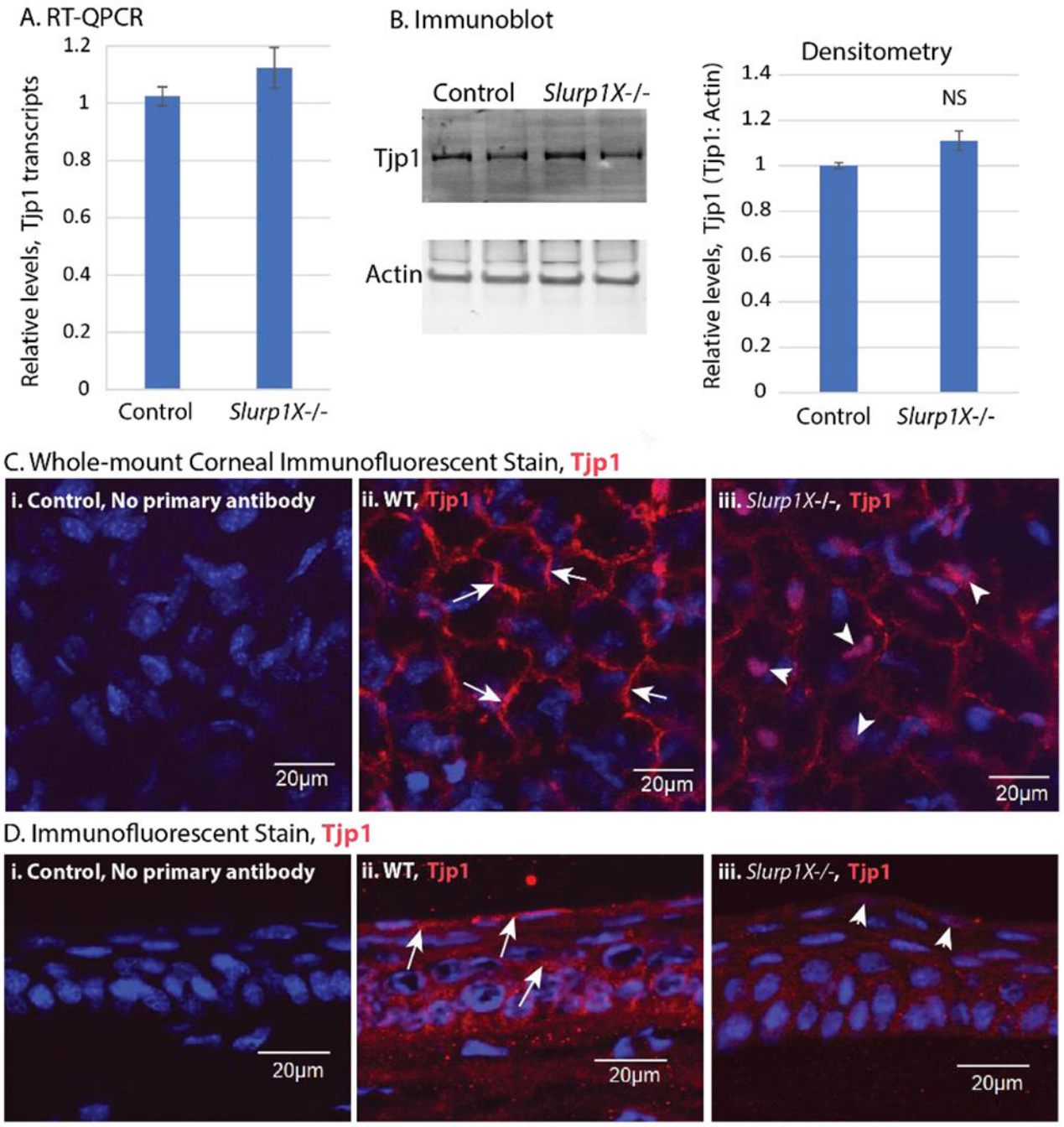

Figure 7. Expression of Tjp1 in the *Slurp1X*−/− mouse CE.

A. RT-QPCR performed using total RNA isolated from dissected WT and *Slurp1X*−/− mouse corneas revealed no difference in relative levels of Tjp1 transcripts (n=10). B. Immunoblots. WT and *Slurp1X*−/− corneal lysates prepared using urea buffer were separated by SDS-PAGE, electroblotted to PVDF membranes and probed with specific antibodies indicated revealed no significant change in Tjp1 expression in the *Slurp1X*−/− corneas (n=6). C. Whole-mount corneal immunofluorescent staining elucidated that TJP1 is properly localized to the cell membranes in the WT CE (arrows), but mis-localized to

the nuclei (arrowheads) in the superficial *Slurp1X*−/− CE cells. Magnification: 40X; Scale bar, 20 μm (n=3). D. Immunofluorescent staining using cryosections elucidated decreased membrane localization of Tjp1 in the *Slurp1X*−/− CE cells (arrowheads) compared with the WT (arrows). Magnification: 40X; Scale bar, 20 μm (n=3).

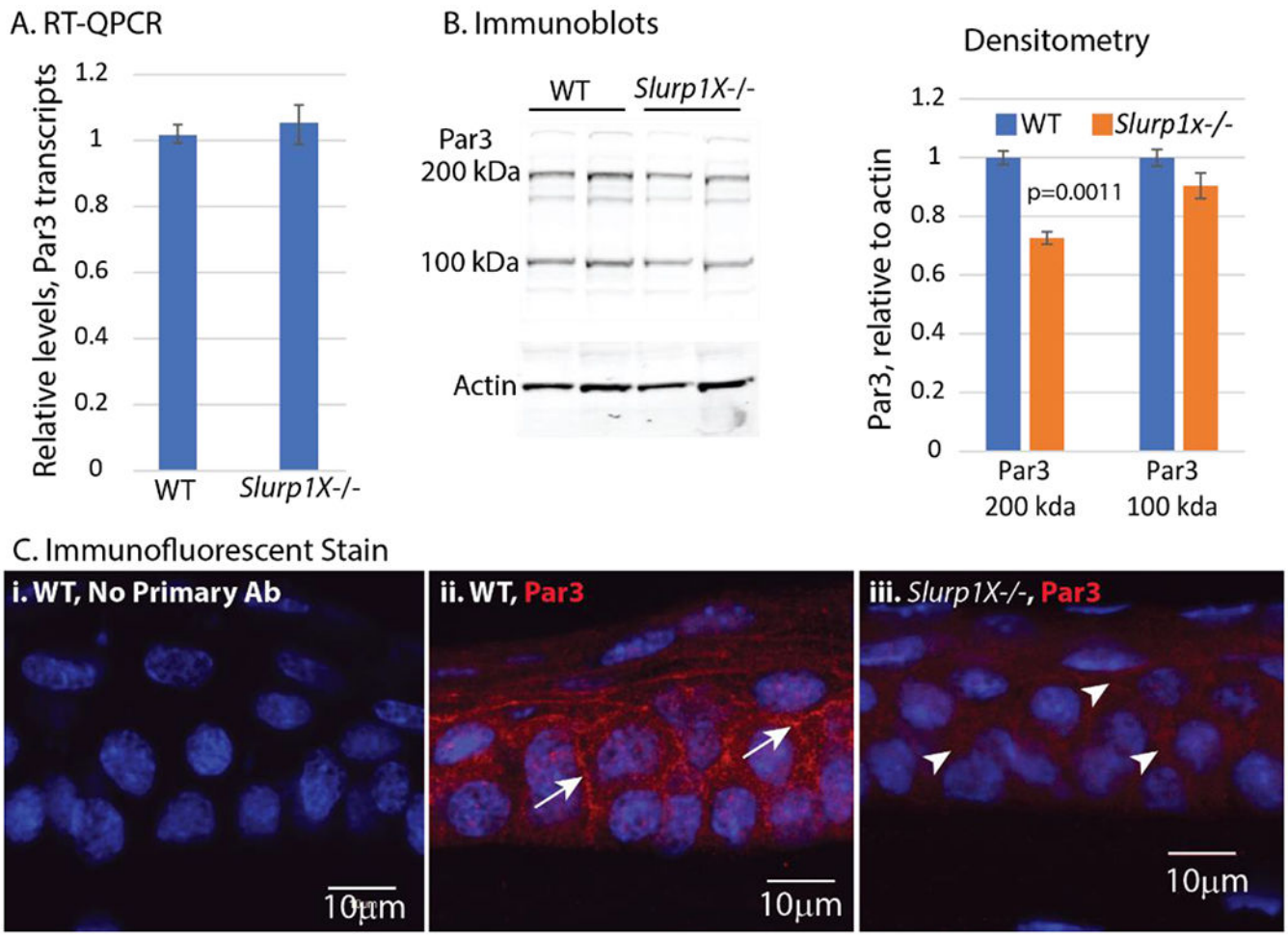

Figure 8. Expression of Par3 in the *Slurp1X*−/− mouse CE.

A. RT-QPCR performed using total RNA isolated from dissected WT and *Slurp1X*−/− mouse corneas revealed no difference in relative levels of *Par3* transcripts (n=7). B. Immunoblots. WT and *Slurp1X*−/− corneal lysates prepared using urea buffer were separated by SDS-PAGE, electroblotted to PVDF membranes and probed with specific antibodies indicated revealed slightly decreased expression of Par3 in the *Slurp1X*−/− corneas (n=6). P values are shown where significant. C. Immunofluorescent staining elucidated that Par3 is localized to the WT CE cell membranes (arrows) while it is localized in a diffuse manner in the *Slurp1X*−/− CE (arrowheads). Magnification: 40X; Scale bar, 10 μm (n=3).

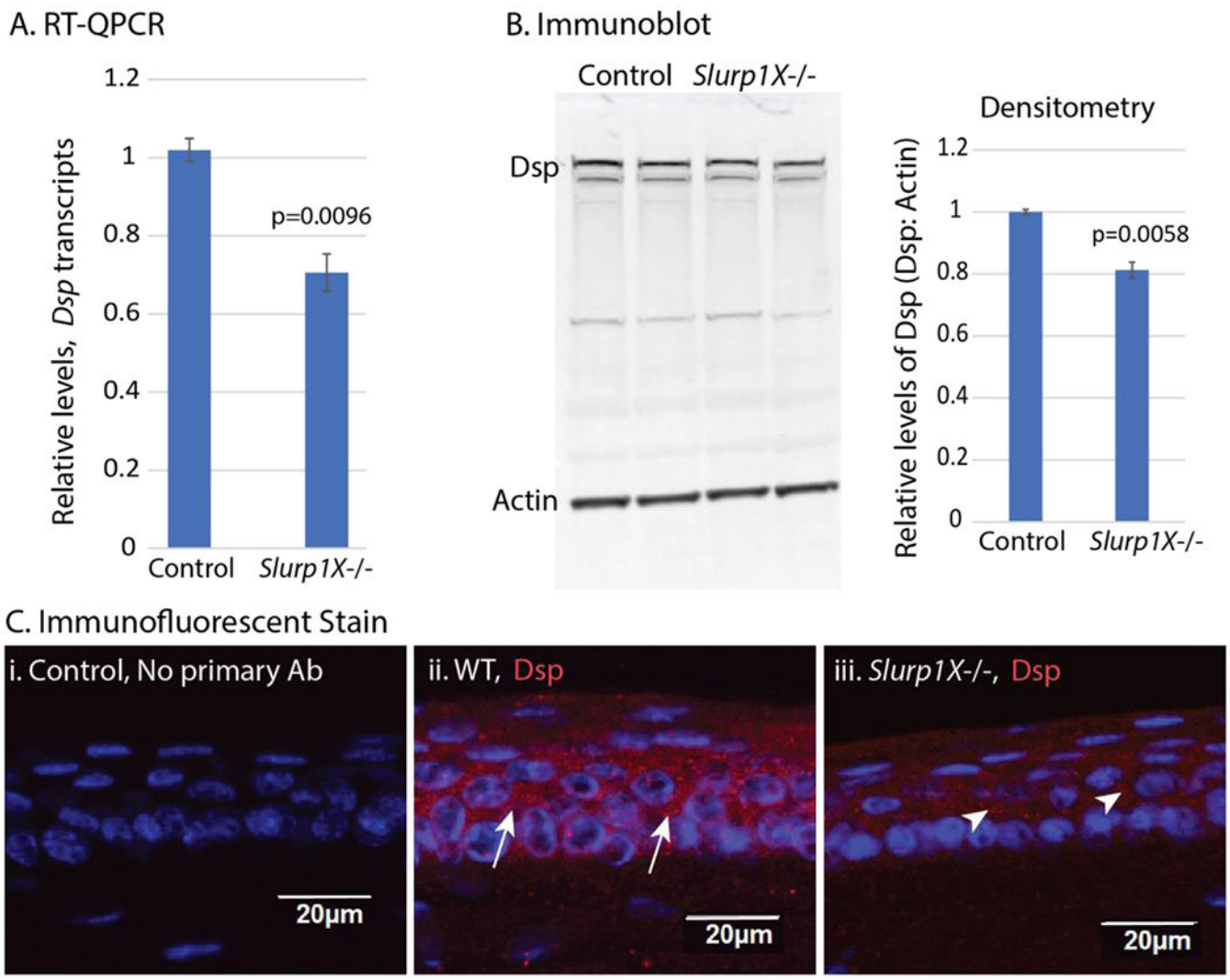

Figure 9. Expression of Dsp in the *Slurp1X*−/− mouse CE.

A. RT-QPCR performed using total RNA isolated from dissected WT and *Slurp1X*−/− mouse corneas revealed a decrease in relative levels of *Dsp* transcripts (n=6). B. Immunoblots. WT and *Slurp1X*−/− corneal lysates prepared using urea buffer were separated by SDS-PAGE, electroblotted to PVDF membranes and probed with specific antibodies indicated revealed slightly decreased expression of Dsp in the *Slurp1X*−/− corneas (n=6). Corresponding p values are shown. C. Immunofluorescent staining elucidated that Dsp is localized to the WT CE cell membranes (arrows) while it is localized in a diffuse manner in the *Slurp1X*−/− CE (arrowheads). Magnification: 40X; Scale bar, 20 μm (n=3).